PERGAMON

International Journal of Heat and Mass Transfer 44 (2001) 3855–3868

International Journal of HEAT and MASS TRANSFER

www.elsevier.com/locate/ijhmt

Numerical study of bottom-wall temperature modulation effects on thermal instability and oscillatory cellular convection in a rectangular enclosure

C.Y. Soong [a,*], P.Y. Tzeng [a], C.D. Hsieh [b]

[a] *Department of Aeronautical Engineering, Rotating Fluids and Vortex Dynamics Laboratory, Chung Cheng Institute of Technology, Tahsi, Taoyuan 33509, Taiwan, ROC*

[b] *Second Division, Chung Shan Institute of Science and Technology, Lungtan, Taoyuan 32507, Taiwan, ROC*

Received 20 June 2000; received in revised form 2 January 2001

Abstract

In the present study, thermal-fluid behaviors in a rectangular enclosure of width-to-height aspect ratio 4:1 heated from below with wall-temperature varied sinusoidally in time is investigated numerically. The main concerns are the effects of the wall-heating modulation on the threshold of thermal instability and the oscillatory cellular convection heat transfer performance at the post-critical conditions. For investigation of heating modulation effects at various conditions, inclination of the enclosure is also considered. The results demonstrate that a bottom-wall temperature modulation of larger amplitude and/or lower frequency generates a relatively stabilizing effect. The trend is the same as those claimed in the previous linear stability analyses of infinite horizontal fluid layer. However, the present numerical solutions further disclosed more detailed information about the flow structure as well as the local heat transfer performance, which are useful in understanding of the modulation mechanisms.

Keywords: Natural convection; Enclosure; Temperature modulation; Oscillatory convection; Thermal instability

1. Introduction

Natural convection in an enclosure always attracts research interests for its academic significance as well as its relevance to wide practical applications. For example, in energy systems, which includes the solar energy collector, nuclear reactor, cryogenic storage, furnace design, heat exchangers, the multi-layered walls and double windows in buildings. They are also found in the solidification and crystal growth of materials processing, the cooling of energy storage components and electronic equipment. Even in the natural environment, buoyancy-driven natural convection appears often, such as in the areas of large-scale meteorology, geophysics and astrophysics. Depending on the orientation of heating and gravity, there are two categories of thermal-buoyancy-induced natural convection in enclosures, one is the so-called *thermally driven flows* and the typical example is the case of side-walls heated differentially, in which the temperature gradient is orthogonal to the buoyancy force. The other one is characterized by a boundary condition of *heated from below*, i.e., the temperature gradient is parallel to the buoyancy force. The latter is usually regarded as a *thermal instability problem* and is often employed as a theoretical or experimental model for investigation of instabilities in non-isothermal fluids. In the past decades, the afore-mentioned two classes of natural convection with steady wall-heating conditions have been investigated extensively, as that shown in review articles such as Ostrach [1] and Yang [2].

Heating condition varying with time is possible in some situations and the associated thermal-flow characteristics become time-dependent. For example, in

* Corresponding author. Tel.: +886-3-390-8102; fax: +886-3-389-1519.

E-mail address: cysoong@ccit.edu.tw http://www.ccit.edu.tw/~RFVDLab (C.Y. Soong).

0017-9310/01/$ - see front matter
PII: S0017-9310(01)00030-8

Nomenclature

As	width-to-height aspect ratio of the enclosure, L/H
f	dimensional frequency (1/s)
g	gravitational acceleration (m/s^2)
Gr	Grashof number, $g\beta\Delta TH^4/\nu^2 L = Ra/(PrAs)$
h, $\bar{h}$	local and average heat transfer coefficients (W/m^2 K)
k	thermal conductivity of fluid (W/m K)
Nu	Nusselt number, hH/k
P	pressure (kPa)
Pr	Prandtl number, ν/α
Ra	Rayleigh number, $g\beta\Delta TH^3/\nu\alpha$
T	local temperature (K)
U, V	velocity components in X and Y directions (m/s)
u, v	dimensionless velocity components in x and y directions
X, Y	Cartesian coordinates (m)
x, y	dimensionless Cartesian coordinates

Greek symbols

α	thermal diffusivity (m^2/s)
β	coefficient of thermal expansion (1/K)
ε	dimensionless amplitude of the temperature modulation
γ	inclined angle of the enclosure (deg)
ν	kinematic viscosity (m^2/s)
ρ	density (kg/m^3)
θ	dimensionless temperature function, $(T - T_c)/\Delta T$
Ψ	dimensionless stream function
τ	dimensionless time
τ_p	dimensionless period of oscillation
ω	dimensionless frequency of the temperature modulation

Subscripts

av	averaged value
c	cold wall or characteristic quantity
h	hot wall
max, min	maximum and maximum value
w	wall condition

electronic equipments the electronic components are frequently energized intermittently and, therefore, generate heat in an unsteady manner. Many investigations have been conducted to study the effects of the transient boundary condition on the side-wall heated enclosures. Effects of step change in side-wall temperature were studied by Patterson and Imberger [3], Nicollete et al. [4], and Schladow et al. [5]. Whereas Yang et al. [6], Kazmierczak and Chinoda [7], and Lage and Bejan [8] studied natural convection in enclosures with oscillatory side-wall temperature. Hyun [9] summarized the previous works and provided a comprehensive review on the subject. Recently, Xia et al. [10] considered the imposed perturbations at the same order of the first natural frequency to a vertical side wall and found that the perturbation destabilizes the flow motion and high amplitude leads to lower critical Rayleigh number for flow starting transition. Kwak and Hyun [11] explored the resonance phenomenon in enclosure with side-wall temperature modulation.

As to the buoyancy-driven convection in an enclosure of bottom-wall with time-dependent wall heating, which is closely related to the present study, early theoretical works on infinitely extended configuration are noteworthy. For an infinite fluid layer confined between two slippery planes and sinusoidally heated from below, Venezian [12] applied linearized analysis to explore the modulating effect on the stability characteristics of mean gradient and claimed that the onset of convection can be delayed by a low frequency of modulation. Later on, Rosentblat and Herbert [13] performed an asymptotic analysis with low-frequency assumption to study the problem of bottom-wall temperature modulation. Rosentblat and Tanaka [14] revealed that the flow field tends to be stabilized at low frequency and high amplitude of modulation. Finucane and Kelly [15], by conducting a nonlinear analysis as well as measurements, claimed that their results present a similar trend as that appearing in the previous analytic works, particularly the amplitude effects of Rosentblat and Tanaka [14]. More comprehensive discussion on modulation effects on thermal instability of fluid layer heated from below can be found in Davis' review article [16] on stability of periodic flows. Ahlers et al. [17] performed a nonlinear analysis by a Lorenz-like low-mode model to study response of the cellular convection to the periodic modulation of the imposed heat current. It was noted that the theoretical results agree well with the experiments. The weakly-nonlinear stability analysis of Roppo et al. [18] showed that the modulation produces a range of stable hexagons near the critical condition. Most recently, Mantle et al. [19] studied modulation effect of bottom-wall heated periodically in time at high Rayleigh number. Comparing with the steady one, they found that the averaged heat transfer can be enhanced by the bottom-wall temperature modulation. Convection resonance and heat transfer enhancement in periodically heated fluid enclosures at high Rayleigh number were recently studied by Lage and Antohe [20].

In the brief review presented above, it is obvious that almost all of theoretical studies on the configuration of *heated from below* were concerned with linear stability

analysis of infinite horizontal fluid layers. For further understanding of the heating modulation effects, however, there are still some topics worthy of study. For example, based on the previous results of linear analysis, we would like to know: (1) Does the heating modulation effects in an enclosure (layer of finite extension) has the same trend? (2) What are the detailed flow structure and temperature field like? (3) Does the heating modulation have significant effects in an inclined enclosure? (4) What are the major influences of modulation effects on the local and overall heat transfer performance? In the present study, a rectangular enclosure of width-to-height aspect ratio 4:1 heated from below with or without inclination is considered. The same configuration but without heating modulation has been employed by Soong et al. [21,22] and Tzeng et al. [23] to study the flow-mode transition phenomena. In this work the attention is focused on the effects of bottom-wall temperature modulation on the threshold of thermal instability as well as flow structure and heat transfer performance under various frequencies and amplitudes. Effects of inclination are also studied to understand the transient response of flow mode transition and heat transfer performance at various inclined angles.

2. Problem statement and governing equations

A two-dimensional inclined rectangular enclosure of height H, length $L = 4H$, and at inclined angle γ is schematically shown in Fig. 1. The two vertical sidewalls are adiabatic, and the fluid is heated from below and cooled at the upper wall. The upper wall is of a constant temperature T_c, and the lower wall is subjected to a temperature oscillatory in time, $T_h(t) = T_{h0} + \varepsilon\Delta T \sin(2\pi ft)$, where T_{h0} stands for the time-mean value of $T_h(t)$ and $\Delta T = T_{h0} - T_c \geqslant 0$ is the characteristic temperature difference; $\varepsilon\Delta T$ and $2\pi f$ are dimensional amplitude and frequency of the oscillation. Characteristic temperature difference ΔT or $\beta\Delta T$, where $\beta = -(1/\rho)(\partial\rho/\partial T)_P$ is the thermal expansion coefficient, is assumed small enough such that Boussinesq approximation is appropriate. The stress-work are very small and can be neglected. The characteristic values of $L_c = H$, $t_c = H^2/\alpha$ and $V_c = \alpha/H$, respectively, are taken as length, time and velocity scales, where α denotes the thermal diffusivity. The dimensionless variables are $\tau = t/t_c$, $(x,y) = (X,Y)/L_c$, $(u,v) = (U,V)/V_c$, and the temperature function is defined as $\theta = (T - T_r)/\Delta T$ and $T_r = T_c$ is the reference temperature. The dimensionless governing equations can be cast into the following form:

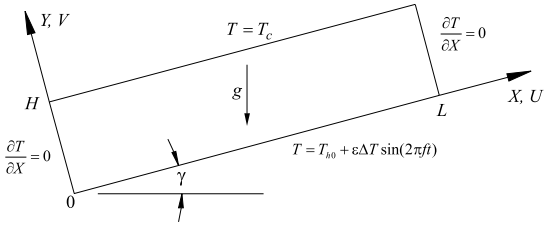

Fig. 1. Physical model and coordinate system.

$$\frac{\partial u}{\partial x} + \frac{\partial v}{\partial y} = 0, \tag{1}$$

$$\frac{\partial u}{\partial \tau} + u\frac{\partial u}{\partial x} + v\frac{\partial u}{\partial y} = Pr\nabla^2 u - \frac{\partial p_d}{\partial x} + Pr\,Ra\sin\gamma\cdot\theta, \tag{2}$$

$$\frac{\partial v}{\partial \tau} + u\frac{\partial v}{\partial x} + v\frac{\partial v}{\partial y} = Pr\nabla^2 v - \frac{\partial p_d}{\partial y} + Pr\,Ra\cos\gamma\cdot\theta, \tag{3}$$

$$\frac{\partial \theta}{\partial \tau} + u\frac{\partial \theta}{\partial x} + v\frac{\partial \theta}{\partial y} = \nabla^2\theta, \tag{4}$$

where $p_d = p - p_r$ is the pressure departure from the reference pressure p_r, $Ra = g\beta\Delta TH^3/\alpha v$ is the Rayleigh number, and v is the kinematic viscosity of the fluid. No-slip condition is imposed at four walls of the enclosure. The boundary conditions in dimensionless form are

$$u = v = 0 \quad \text{at the walls}, \tag{5}$$

$$\partial\theta/\partial x = 0 \quad \text{at } x = 0 \text{ and } x = As, \tag{6}$$

$$\theta = 1 + \varepsilon\sin(2\pi\omega\tau) \quad \text{at } y = 0, \tag{7}$$

$$\theta = 0 \quad \text{at } y = 1, \tag{8}$$

where $As = L/H$ is the width-to-height aspect ratio of the rectangular enclosure; $\tau = t/t_c$, ε and $\omega = ft_c$ are the dimensionless time variable, oscillation amplitude and frequency, respectively; and $\omega\tau = ft$ denotes cycle number of the oscillation.

3. Method of solution

The governing equations, (1)–(4), with the prescribed boundary conditions, (5)–(8), are discretized by using an improved version of QUICK scheme [24] and the resultant difference equations are solved by SIMPLEC algorithm [25]. The grid system used in the present computation is of staggered and uniform distributions. Crank–Nicolson implicit scheme is applied for the discretization of time derivatives. The convergence criterion at each time instant is $|\phi^{k+1}_{max} - \phi^{k}_{max}/\phi^{k+1}_{max}| \leqslant 10^{-4}$, where ϕ denotes the dependent variables, i.e., u, v and θ. The steady state is reached while the relative deviation between values of each variable at two consecutive time-steps is less than 10^{-5}. All of the computations are performed on HP/755 workstations.

To check the validity of the present numerical procedure, the thermally driven low-Pr fluid flow by sidewall heating in an enclosure of $As = 4$ is taken as a case examined. The natural convection problem was solved

by a variety of numerical methods and discussed at the GAMM-Workshop [26]. The case of rigid upper surface (i.e., the so-called R–R Case), $Gr = 3 \times 10^4$ (or $Ra = 1800$) and $Pr = 0.015$ is selected in the present numerical test, where Gr is Grashof number and is defined as $Gr = g\beta\Delta TH^4/v^2L = Ra/PrAs$. The time step used in the present test is 10^{-4}. Tables 1 and 2 show comparisons of the solver and the results of the present work with some of the numerical results presented at the GAMM-Workshop [26]. Most of the computations, including the present one, employ a high-order scheme for this problem. It is observed that the fluid motion at $Gr = 3 \times 10^4$ is not steady but oscillating in nature. Time history of the characteristic quantities presented in Table 2 are defined as follows: $U_{\max}(U_{\min}) =$ maximum (minimum) value of $|U|$ at $X = L/4$, $V_{\max}(V_{\min}) =$ maximum (minimum) value of $|V|$ at $Y = H/2$, $\Psi_{\max}(\Psi_{\min}) =$ maximum (minimum) value of $|\Psi|$ and f_r denotes the response frequency of the fluids, where Ψ is the stream function.

Table 2 shows the comparisons of the present results with those of the studies listed in Table 1. Among them, Benhnia and de Vahl Davis' results on the finest grid of 321×81 points is considered as a benchmark. Although the present max–min values of local velocities deviate from the benchmark results, they lie in a reasonable range spanned by the others. It is most noteworthy that the response frequency, which is one of the important characteristics of oscillatory flows, generated by the present computation is very close to the benchmark and is the best on the list. As to the other two flow quantities, $\Psi_{\max}$ and $\Psi_{\min}$, related to the strength of the vortices, the present predictions are of only 3.5% and 3.0% deviations, respectively. Generally speaking, the present third-order QUICK computations on the grid of 81×21 points is appropriate for considerations of accuracy as well as saving the computational efforts.

4. Results and discussion

4.1. Critical Rayleigh number for zero modulation

Theoretical analyses have shown that the critical Rayleigh number for the onset of convection for a horizontal infinite layer heated from below is $Ra_c = 1708$. In the present study, the configuration is no longer infinite but confined by two vertical walls. According to the results of the previous studies, e.g., [27], the boundary effects on the critical condition become small and the critical Rayleigh number approaches the above theoretical value as As increases. A rectangular enclosure of $As = 4$ is considered in the

Table 1
Comparison of numerical methods with some contributors at the GAMM-Workshop [26]

Authors	Space	Time	Algorithm
Behnia and de Vahl Davis (pp. 11–18)[a]	Second-order Cent. Diff.	Forward Diff.	Samarskii–Andreyev ADI
Ben Hadid and Roux (pp. 25–34)	Hermitian Method	ADI	Finite Diff.
Desrayaud et al. (pp. 49–56)	Second-order Cent. Diff.	ADI	Finite Diff.
Grotzbach (pp. 57–64)	Schmann's Method (second-order)	Explicit Euler Leap Frog (second-order)	3D TURBIT
Maekawa and Doi (pp. 74–81)	Cent. Diff. for Hor., QUICK for Ver.	Euler Explicit (first-order)	ICE With MILUBCG
Ohshima and Ninokata (pp. 82–89)	QUICK (second-order)	ICE (second-order)	AQUA
Present	QUICK (third-order)	Crank–Nicolson implicit (second-order)	SIMPLEC

[a] Page numbers here are the papers appeared in [26].

Table 2
Comparison of computational results for natural convection in a horizontal enclosure ($\gamma = 0°$) of 4:1 at $Gr = 3 \times 10^4$, $Pr = 0.015$ [26][a]

Authors	Girds	$U_{\min}$	$U_{\max}$	$V_{\min}$	$V_{\max}$	$\Psi_{\min}$	$\Psi_{\max}$	f_o
Behnia and de Vahl Davis	321×81, Unif.	0.4319	0.8411	0.4895	0.9526	0.4291	0.4723	18.05
Ben Hadid and Roux	121×41, Non-Unif.	0.5168	0.7744	0.5900	0.8747	–	–	18.18
Desrayaud et al.	101×33, Unif.	0.5146	0.7266	0.6024	0.8286	0.4401	0.4593	17.89
Grotzbach	$16 \times 4 \times 34$, Unif.	–	0.6305	–	0.7411	–	–	18.09
Maekawa and Doi	80×20, Unif.	0.596	0.662	0.685	0.754	–	–	17.9
Ohshima and Ninokata	81×21, Unif.	0.558	0.645	0.656	0.762	–	–	18.1
Present	81×21, Unif.	0.5574	0.6882	0.6448	0.7963	0.4441	0.4579	18.08

[a] $f_o =$ oscillation frequency without modulation.

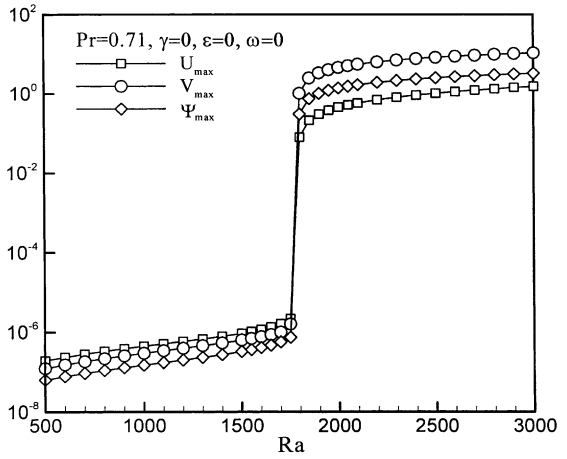

Fig. 2. The values of U_{max}, V_{max} and Ψ_{max} at various Ra.

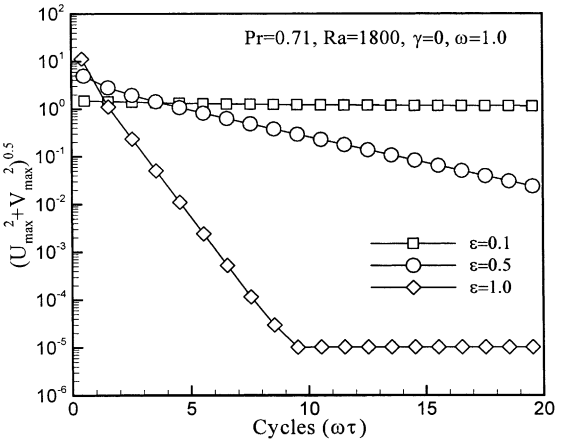

Fig. 3. Time history of mean maximum velocity at various modulation amplitudes.

present numerical computations. Fig. 2 displays the computational results of U_{max}, V_{max} and Ψ_{max} at different Rayleigh numbers. The results show that U_{max}, V_{max} and Ψ_{max} slightly increase for $Ra < 1800$ and almost maintain at the order of 10^{-7}. However, a sudden jump from the order about 10^{-6} to 10^{-1} appears at $Ra = 1800$, then followed by an ascending trend with Ra increasing. This jump implies a bifurcation of flow state from a stationary and conduction state to a cellular convection one. The computations are always performed from low Ra to a higher one and the increment is 50 near the critical condition. The bifurcation occurs at Ra between 1750 and 1800. Performing successive computations in this Ra range with increment of $\Delta Ra = 10$ finds that the critical Rayleigh number Ra_{c0} is around 1780 for this case of $As = 4$ without bottom-wall heating modulation. Comparing with the theoretical value of 1708 for infinite fluid layer, the present value is higher due to the stabilizing effect in the presence of the side-wall confinement.

4.2. Effect of imposed modulation on onset of convection

As the bottom-wall temperature modulation is applied, the temperature oscillation influences fluid flow and heat transfer characteristics in the enclosure. The responses of the maximum values of velocity, U_{max} and V_{max}, in the enclosure are fluctuating with the wall-temperature at each cycles. In Fig. 3, a parameter characterizing the maximum velocity, $(U_{max}^2 + V_{max}^2)^{0.5}$, at $Ra = 1800$, $\gamma = 0$ and $\omega = 1.0$ are plotted and used to illustrate the amplitude effects of imposed temperature modulation. For this configuration of $As = 4$ at $Ra = 1800$, the onset of thermal instability has been triggered and the fluid motion is of a cellular pattern. As shown in Fig. 3, weak modulation of small amplitude, $\varepsilon = 0.1$, seems less influential on the velocity field. With $\varepsilon = 0.5$, however, the values of $(U_{max}^2 + V_{max}^2)^{0.5}$ decay with number of modulation cycle in, at least, 20 cycles computed and presented. With a large amplitude, $\varepsilon = 1.0$, the decaying rate of velocity becomes fast. After 10 cycles, the maximum velocity has decayed to the order of 10^{-6} and maintained almost constant. It is an evidence of the stabilizing effect by the bottom-wall temperature modulation of high amplitude.

The modulation effects with different oscillation frequencies are shown in Fig. 4 for $Ra = 1800$, $\gamma = 0$ and $\varepsilon = 1.0$. At low frequency, $\omega = 0.1$, the maximum velocity of the cellular flow is of order O(10) and it seems almost constant under the modulation. As the modulation frequency increases to $\omega = 0.5$, the flow tends to settle down quickly to a velocity of order 10^{-4} in only 5 cycles. At $\omega = 1.0$, the velocity decays to order

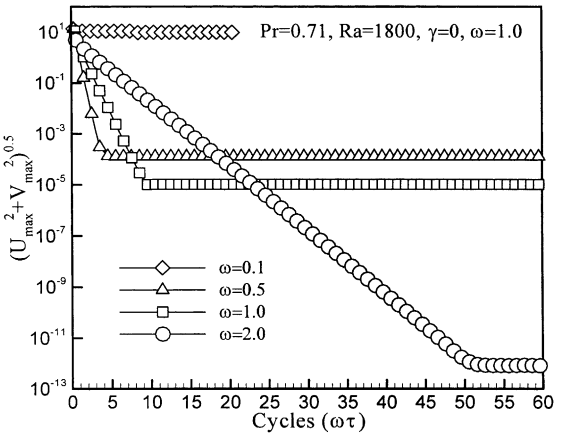

Fig. 4. Time history of mean maximum velocity at various modulation frequencies.

of 10^{-5} at 10 cycles. At high frequency, $\omega = 2.0$, the velocity decay sustains within 50 cycles and then settles down. The response of the fluid motion to the suppression of modulation with low frequency is faster. The relatively larger frequency may result in slower decaying but the mean fluid motion seems to be suppressed to a lower level. In. Fig. 2, it is known that the velocity components at $Ra = 1800$ are of the order of $O(10^{-1})$–$O(1)$. The maximum velocities of $O(10^{-4}$–$10^{-12})$ at the large frequencies in Fig. 4 are all small enough. Therefore, the onset of the convection can be regarded as being suppressed at $\omega \geqslant 0.5$.

Fig. 5 illustrates flow characteristics with wall-temperature modulation of $\varepsilon = 1.0$ and $\omega = 1.0$ at different Rayleigh numbers. With increasing Rayleigh number, the rate of velocity decay becomes slow. In the cases studied, the modulation provides stabilizing effect on the flow field. For $Ra \geqslant 2100$, the stabilizing effect diminishes. Comparing to the critical Rayleigh number for stationary case, $Ra_{c0} = 1780$, the onset of thermal instability under the modulation of $\varepsilon = 1.0$ and $\omega = 1.0$ occurs at $Ra_c = 2050$. An index defined as $(Ra_c - Ra_{c0})/Ra_{c0}$ is used to characterize the stabilizing effect of the temperature modulation, and it is 16.67% for the case mentioned above. The plot of $(Ra_c - Ra_{c0})/Ra_{c0}$ versus amplitude ε for $\gamma = 0$ and $\omega = 1$ is displayed in Fig. 6. The value of $(Ra_c - Ra_{c0})/Ra_{c0}$ increases with the amplitude ε, which implies that the modulation of high amplitude gives better performance in delaying the onset of convection. While it is seen in Fig. 7 that the value of $(Ra_c - Ra_{c0})/Ra_{c0}$ decreases with the increasing ω. With the aid of the order-of-magnitude of mean velocity in Fig. 4, it can be inferred that the imposed temperature modulation of lower frequency delays the onset of convection more efficiently.

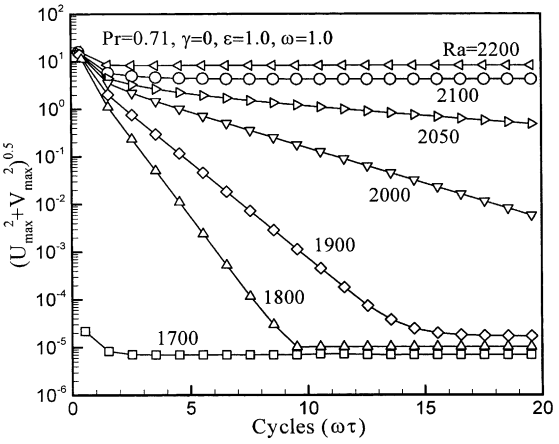

Fig. 5. Time history of mean maximum velocity at various *Ra*.

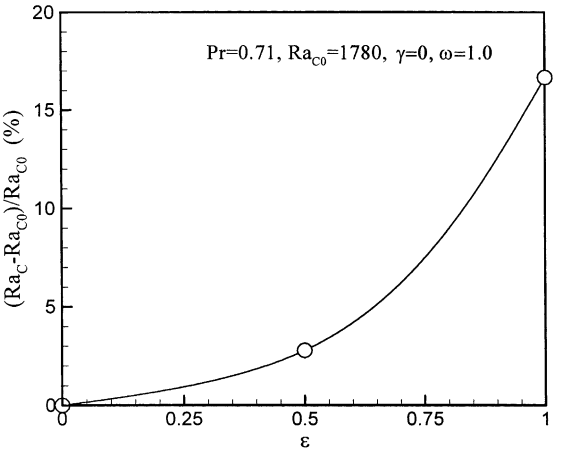

Fig. 6. Effects of modulation amplitude on the critical condition.

Except that of extremely low frequency, e.g., $\omega = 0.1$ and $Ra = 1800$, the above observations indicate that, in general, the bottom-wall temperature modulation of large amplitude and low frequency may stabilize the fluid motion in a horizontal enclosure. The similar nature can be found in studies of other flow systems, e.g., an early experiment on the fluid confined in the narrow gap between two cylinders with rotation modulation of the inner cylinder conducted by Donnely and Schwart [28]. Just the same as the present study, he revealed that a large-amplitude modulation results in a stronger stabilizing effect. The Rayleigh–Benard thermal instability has an analogy to the Taylor instability, Venezian [12] and Rosentblat and Herbert [13] also concluded the same trend in their theoretical studies of thermal instability.

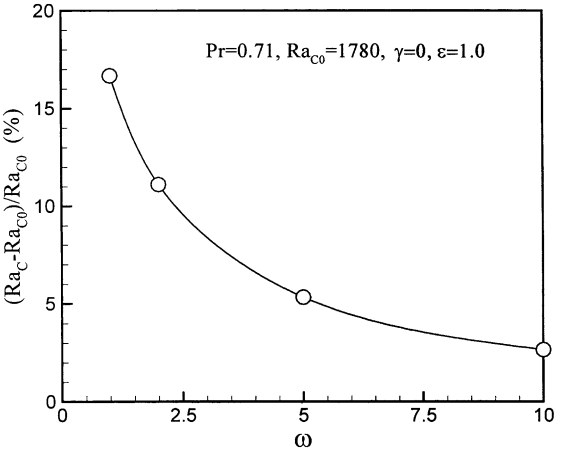

Fig. 7. Effects of modulation frequency on the critical condition.

4.3. Effect of imposed modulation and inclination on thermal flow fields

As the heated enclosure is inclined at an angle γ as shown in Fig. 1, the convection flow in the enclosure easily starts moving even at very low Rayleigh number for the presence of the unbalanced buoyancy effects on the up-slope (heated) and down-slope (cooled) surfaces. One objective of the present study is to investigate the effect of imposed wall-temperature modulation on flow field in an inclined enclosure. In this part, numerical computations for cellular convection in an enclosure with bottom wall ($y = 0$) temperature modulation at various inclined angles is performed.

The streamlines and isotherms at $Ra = 2000$ with and without imposed wall-temperature modulation of $\varepsilon = 1$ and $\omega = 1$, are shown in Figs. 8–13 for $\gamma = 1°, 5°, 15°, 25°, 50°$ and 90°, respectively. In these figures, the steady state (SS) shown in subplot (a) denotes thermal fluid solutions without modulation and is used as initial condition in the computations. The subplots (b)–(e) show the corresponding four phases at $\tau = 0$, $1/4\tau_p$, $2/4\tau_p$, and $3/4\tau_p$ of a fully developed modulation cycle, i.e., after at least 10 cycles. The parameter τ_p stands for the dimensionless period of the temperature modulation. In Fig. 8(a), the enclosure inclined at $\gamma = 1°$, the flow structure of the enclosure appears four cells. The thermal flow under the influences of imposed wall-temperature modulation at various inclined angles is calculated by employing the steady-state solutions as the initial condition. After a transient stage of several cycles, the flow and temperature fields will become an oscillatory state of fully developed periodicity for this value of Ra. The flow patterns are two-cell mode as the bottom-wall temperature $\theta_h = 2.0$ at $\tau = 1/4\tau_p$ as shown in the isotherms in Fig. 8(b). In this situation, the bottom wall has the peak value and the largest temperature difference in a modulation cycle. The strong buoyancy effect in the enclosure generates vorticity in the cellular flow, where the strength of the cellular motion is characterized by

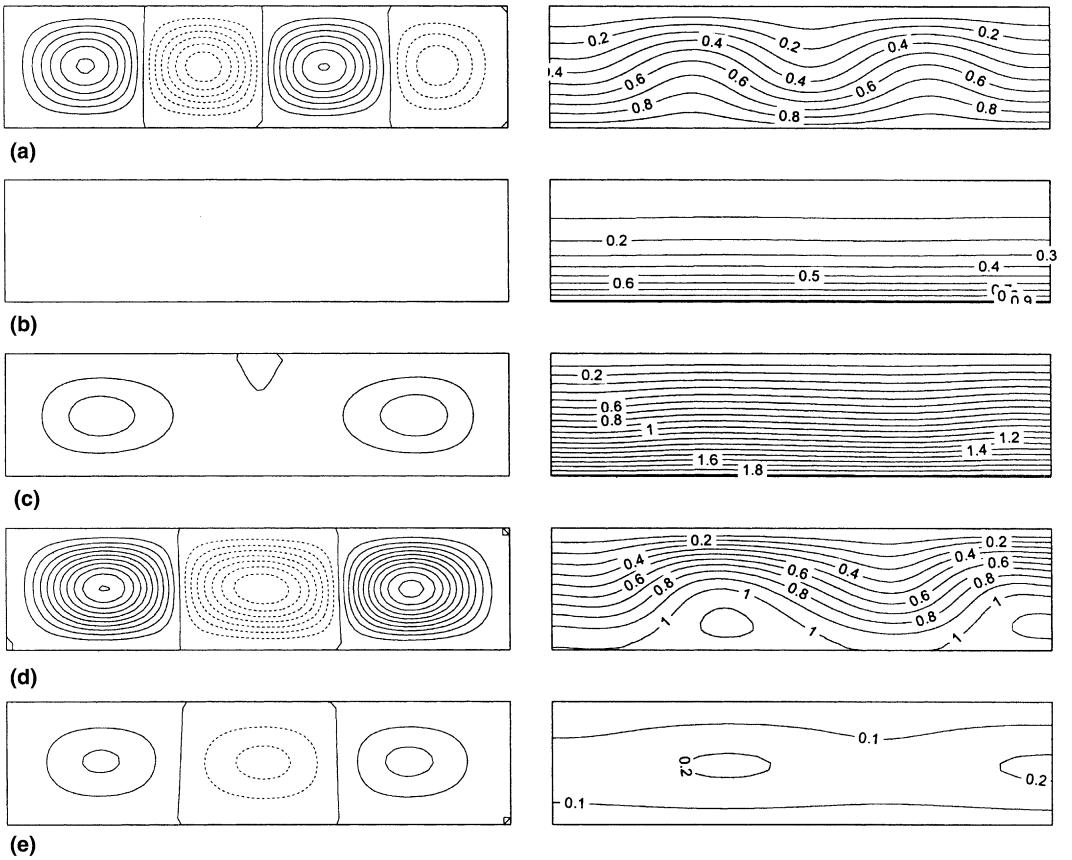

Fig. 8. Streamlines and isotherms for the case of $Pr = 0.71$, $Ra = 2000$, $\gamma = 1°$, $\varepsilon = 1.0$ and $\omega = 1.0$. (a) Steady state (SS) as initial condition of the computation, $\theta_h = 1.0$, $-1.355 \leqslant \Psi \leqslant 1.415$, $0 \leqslant \theta \leqslant 0.982$; and oscillatory solutions at (b) $\tau = 0$, $\theta_h = 1.0$, $0 \leqslant \Psi \leqslant 0.092$, $0 \leqslant \theta \leqslant 1.0$; (c) $\tau = 1/4\tau_p$, $\theta_h = 2.0$, $0 \leqslant \Psi \leqslant 0.506$, $0 \leqslant \theta \leqslant 2.0$, (d) $\tau = 2/4\tau_p$, $\theta_h = 1.0$, $-1.585 \leqslant \Psi \leqslant 2.084$, $0 \leqslant \theta \leqslant 1.0$; and (e) $\tau = 3/4\tau_p$, $\theta_h = 0$, $-0.471 \leqslant \Psi \leqslant 0.454$, $0 \leqslant \theta \leqslant 0.212$.

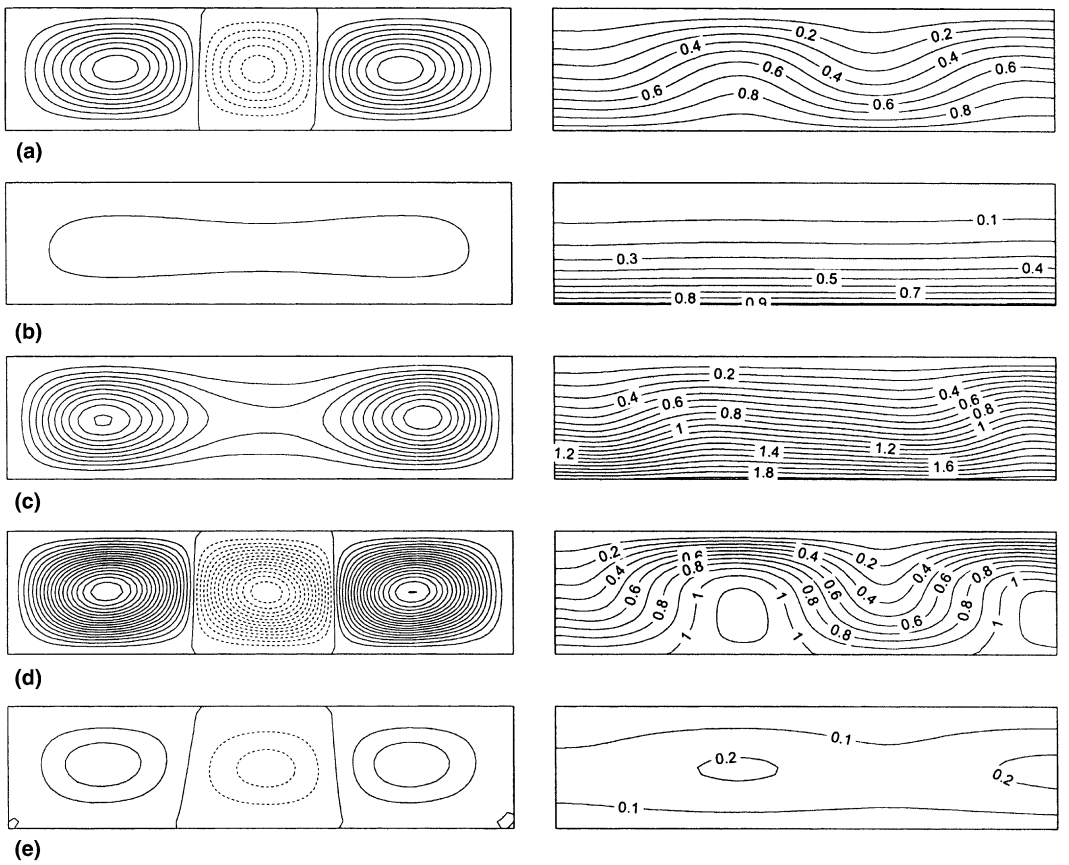

Fig. 9. Streamlines and isotherms for the case of $Pr = 0.71$, $Ra = 2000$, $\gamma = 5°$, $\varepsilon = 1.0$ and $\omega = 1.0$. (a) Steady state (SS) as initial condition of the computation, $\theta_h = 1.0$, $-1.112 \leqslant \Psi \leqslant 1.764$, $0 \leqslant \theta \leqslant 1.0$; and oscillatory solutions at (b) $\tau = 0$, $\theta_h = 1.0$, $0 \leqslant \Psi \leqslant 0.350$, $0 \leqslant \theta \leqslant 1.0$; (c) $\tau = 1/4\tau_p$, $\theta_h = 2.0$, $0 \leqslant \Psi \leqslant 2.159$, $0 \leqslant \theta \leqslant 2.0$; (d) $\tau = 2/4\tau_p$, $\theta_h = 1.0$, $-2.775 \leqslant \Psi \leqslant 3.609$, $0 \leqslant \theta \leqslant 1.187$; and (e) $\tau = 3/4\tau_p$, $\theta_h = 0$, $-0.494 \leqslant \Psi \leqslant 0.545$, $0 \leqslant \theta \leqslant 0.219$.

the absolute value of the stream-function. It is observed that the flow is accelerating due to the vorticity enhancement and transits to three-cell structure at $\tau = 2/4\tau_p$, as shown in Fig. 8(d). As $\tau > 1/4\tau_p$, the wall-temperature is decreasing and the vorticity, which supplied by the buoyancy effect, is also decreasing. As shown in Fig. 8(e), at $\tau = 3/4\tau_p$, the strength of the three cells in the enclosure become weak and then turn to almost stationary at $\tau = 4/4\tau_p$ or $\tau = 0$ in Fig. 8(a). For a new cycle, the wall-temperature and thus the buoyancy force are increasing as $\tau > 0$ and the flow vorticity is generated. Therefore, the flow begins accelerating and forms two-cell and, then, three-cell structure. The flow field transition is repeated cycle by cycle due to the wall temperature modulation.

As the inclined angle increasing, the flow mode transition occurs, i.e., three-cell structure at $\gamma = 5°$ in Fig. 9(a), two-in-one cell mode at $\gamma = 15°, 25°$ and $50°$, as illustrated in Figs. 10(a), 11(a), and 12(a), respectively. At the further high inclination up to $\gamma = 90°$, Fig. 13(a), the flow fields are of uni-cell mode somewhat similar to that at 50°. Effects of inclination on the flow mode transition without modulation has been attacked in detail in a previous work by Soong et al. [22]. With the increasing inclination, the flow structure becomes simpler with the number of the cells reduced, but the strength of the cellular motion can be enhanced and secondary vortices may be induced in the corner regions. In Figs. 8–13, it is also observed that the absolute value of the maximum stream-function or the strength of the cellular motion increases with the inclination. The influences of the temperature modulation on the flow structure and isotherm patterns become less apparent at large inclined angles. Table 3 summarizes the flow mode transition at various inclined angles, where "C" designates the vortex cell producing in the enclosure and "S" denotes the secondary vortex appearing at corners. In Table 3, it is noted that the number of the vortex cells reduces with increasing inclination but the induced secondary vortex occurs and

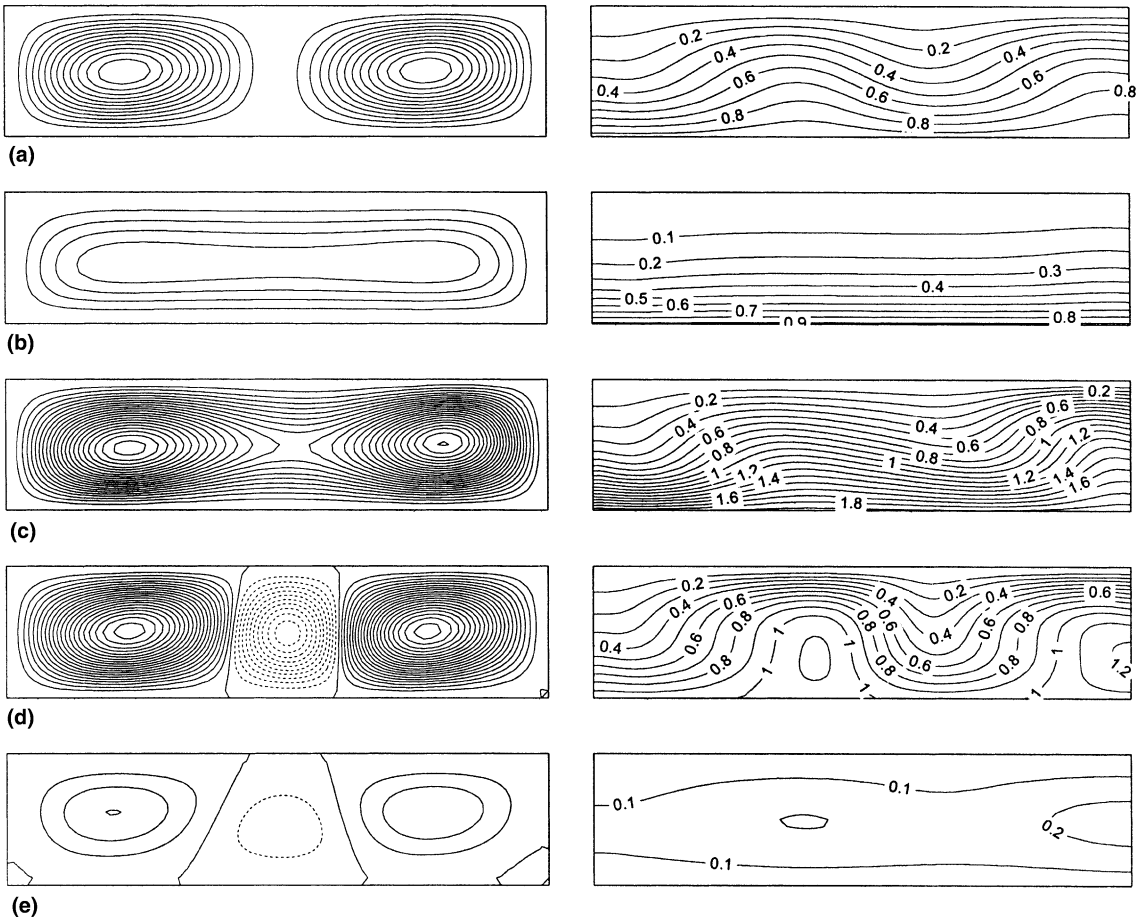

Fig. 10. Streamlines and isotherms for the case of $Pr = 0.71$, $Ra = 2000$, $\gamma = 15°$, $\varepsilon = 1.0$ and $\omega = 1.0$. (a) Steady state (SS) as initial condition of the computation, $\theta_h = 1.0$, $0 \leqslant \Psi \leqslant 2.584$, $0 \leqslant \theta \leqslant 1.0$; and oscillatory solutions at (b) $\tau = 0$, $\theta_h = 1.0$, $0 \leqslant \Psi \leqslant 0.976$, $0 \leqslant \theta \leqslant 1.0$; (c) $\tau = 1/4\tau_p$, $\theta_h = 2.0$, $0 \leqslant \Psi \leqslant 4.622$, $0 \leqslant \theta \leqslant 2.0$; (d) $\tau = 2/4\tau_p$, $\theta_h = 1.0$, $-2.150 \leqslant \Psi \leqslant 4.115$, $0 \leqslant \theta \leqslant 1.222$; and (e) $\tau = 3/4\tau_p$, $\theta_h = 0$, $-0.351 \leqslant \Psi \leqslant 0.605$, $0 \leqslant \theta \leqslant 0.231$.

grows, see also the corresponding flow patterns shown in Figs. 8–13.

4.4. Responses of the local temperature

In order to understand the difference in local responses, it is very significant to examine the local temperature variations under the condition of bottom-wall temperature modulation. Nine locations at which the variations of local temperature to be examined are shown in Fig. 14(a), i.e., $\theta_1(x, y) = (0, 0.25)$, $\theta_2(0, 0.5)$, $\theta_3(0, 0.75)$, $\theta_4(0.5, 0.25)$, $\theta_5(0.5, 0.5)$, $\theta_6(0.5, 0.75)$, $\theta_7(1, 0.25)$, $\theta_8(1, 0.5)$, and $\theta_9(1, 0.75)$, are examined. For generality, a case of inclined enclosure at $Ra = 2000$ and $\gamma = 15°, \varepsilon = 1.0$ and $\omega = 1.0$ in Fig. 14(b) is considered. The forcing function of the bottom-wall temperature, θ_h, is also plotted as a reference. It is observed that, at the same station of $x =$ constant, the responses at the locations near the bottom-wall, i.e., θ_1, θ_4 and θ_7, are of larger amplitudes and less phase-lag since their locations are close to the source of the temperature modulation at $y = 0$. On a line of $y =$ constant, e.g., the line of $y = 0.5$, the temperature at the leftmost (low end) location, θ_2, shows relatively more obvious temperature oscillation; while that at the rightmost (highest end) on the same line, θ_8, is of least phase-lag. In summary, modulation effects are more remarkable in the area of the down-left corner, e.g., the locations of θ_1, θ_2 and θ_4 in Fig. 14(a). Noticeable phase-lag appears on the centerline of $x = 0.5$; whereas the local temperature responses on the line of $x = 1.0$ are almost in phase with (or of one-period lag) the forcing modulation.

In examining the corresponding flow patterns at $\gamma = 15°$ shown in Fig. 10, it is found that, at time around $\tau = 3/4\tau_p$, the cellular motion is relatively weak and the

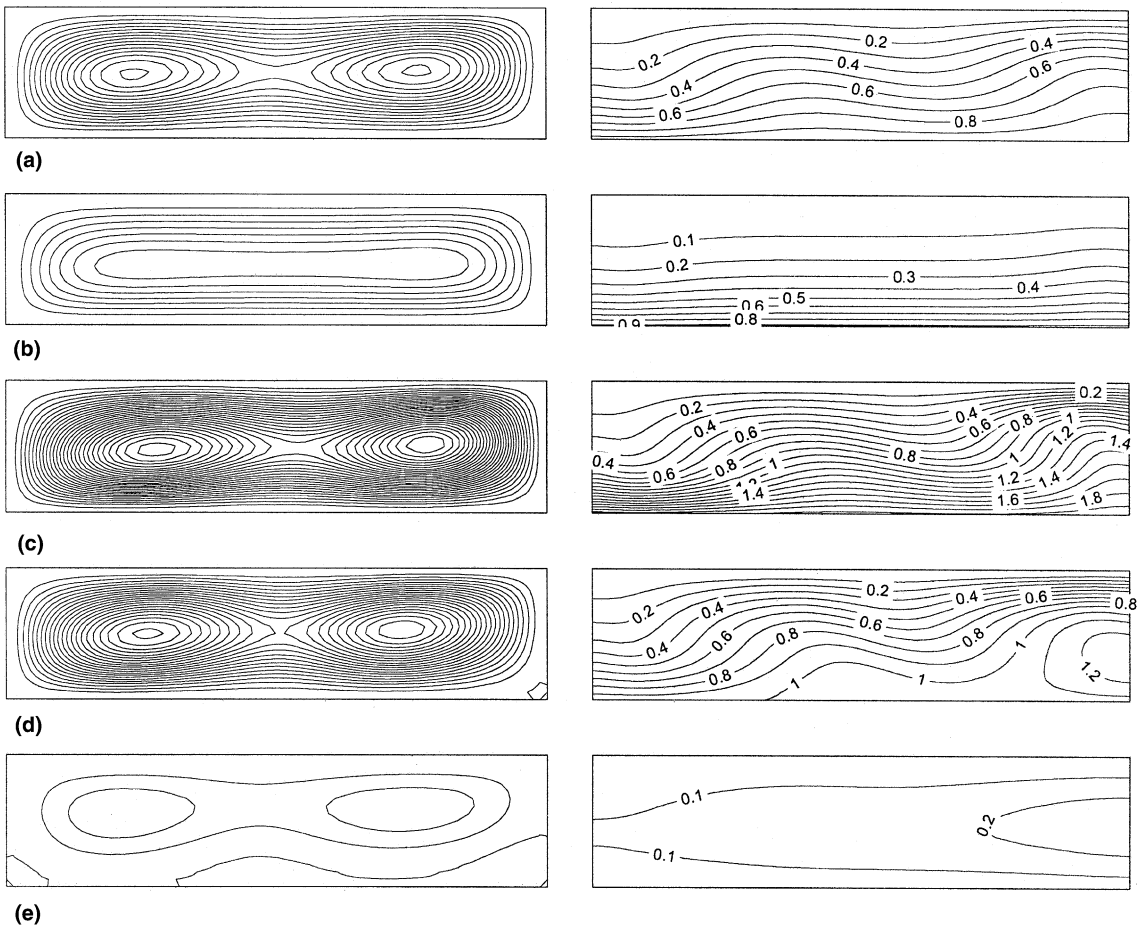

Fig. 11. Streamlines and isotherms for the case of $Pr = 0.71$, $Ra = 2000$, $\gamma = 25°$, $\varepsilon = 1.0$ and $\omega = 1.0$. (a) Steady state (SS) as initial condition of the computation, $\theta_h = 1.0$, $0 \leqslant \Psi \leqslant 3.045$, $0 \leqslant \theta \leqslant 1.0$; and oscillatory solutions at (b) $\tau = 0$, $\theta_h = 1.0$, $0 \leqslant \Psi \leqslant 0.157$, $0 \leqslant \theta \leqslant 1.0$; (c) $\tau = 1/4\tau_p$, $\theta_h = 2.0$, $0 \leqslant \Psi \leqslant 5.765$, $0 \leqslant \theta \leqslant 2.0$; (d) $\tau = 2/4\tau_p$, $\theta_h = 1.0$, $0 \leqslant \Psi \leqslant 4.266$, $0 \leqslant \theta \leqslant 1.267$; and (e) $\tau = 3/4\tau_p$, $\theta_h = 0$, $-0.039 \leqslant \Psi \leqslant 0.573$, $0 \leqslant \theta \leqslant 0.256$.

temperature gradient in the whole is quite small. In Fig. 14, the temperature responses at the nine typical locations display a common feature, i.e., the difference in local temperatures diminishes in the course of θ_h decreasing. All the local temperatures tend to approach the temporal value of the bottom-wall temperature, θ_h, at an instant around $\tau = 0.82\tau_p$. It is noted that the local temperature differences are small and then the buoyancy is weak in the period of $\tau = 0.7\tau_p$ to $0.85\tau_p$. This thermal characteristic underlies the relative weakness of the cellular flow shown at $\tau = 3/4\tau_p$. The flow behaviors in the cases at the other inclined angles have the similar nature, see Figs. 8–13.

4.5. Modulation effects on heat transfer rates

Fig. 15 shows the time series of averaged heat transfer rate on the hot wall ($y = 0$) and the cold wall ($y = 1$). The average Nusselt number, Nu_{av}, is calculated by using Simpson's rule for numerical integration over the wall. By comparing with the forcing oscillation of the bottom-wall temperature, either the hot and cold walls are out of phase. The presence of the phase leading and lag implies that the fluids need time to reflect the variation of the bottom-wall temperature. It is noted that the situation is different from the stationary case, in which the heat transfer rates on the bottom and top walls are balanced. In this oscillatory case, the instantaneous difference between the heat transfer rates of bottom-wall and the top-wall is attributed to the transient enthalpy change of fluids in the enclosure. Fig. 16 illustrates the phase leading and lag of averaged Nusselt numbers at various inclined angles. The phase leading and lag become small and approach constant values with increasing inclined angles. Due to the strong cellular motion in the en-

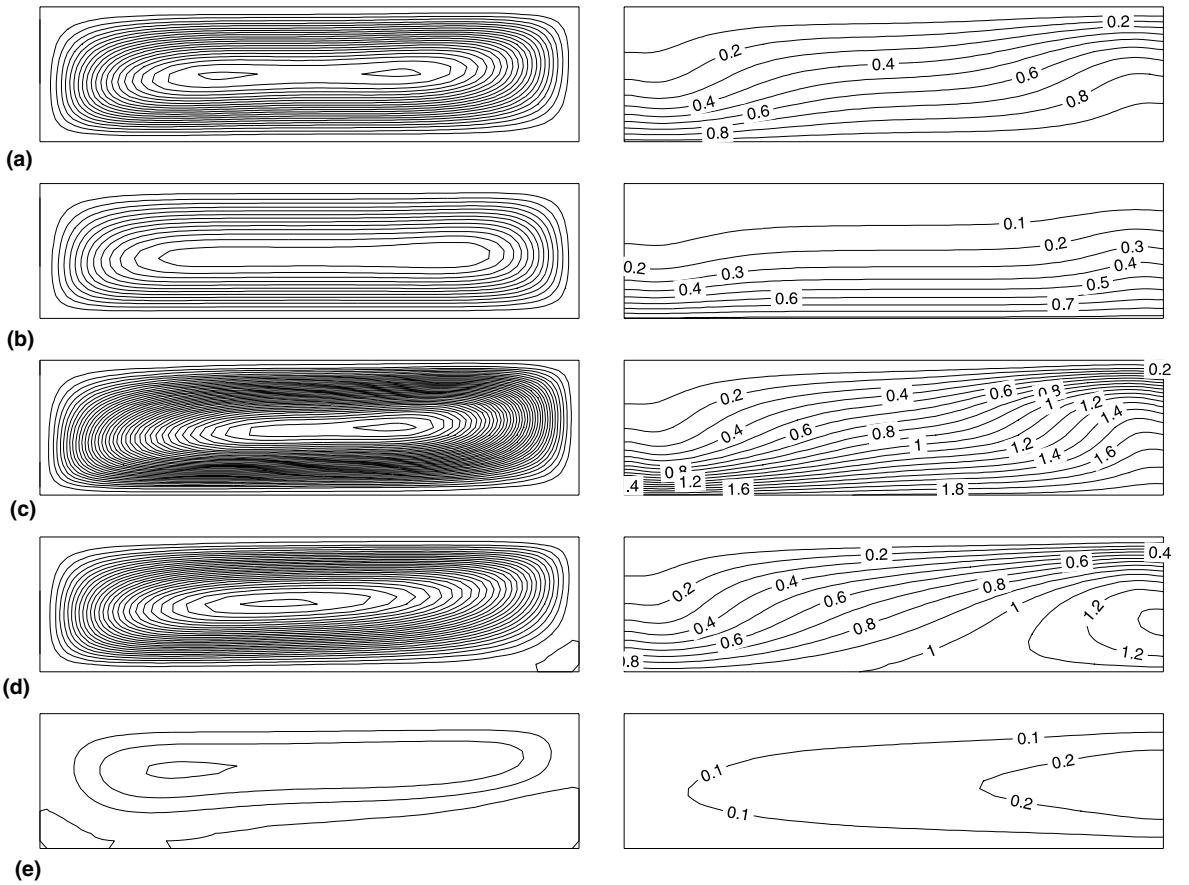

Fig. 12. Streamlines and isotherms for the case of $Pr = 0.71$, $Ra = 2000$, $\gamma = 50°$, $\varepsilon = 1.0$ and $\omega = 1.0$. (a) Steady state (SS) as initial condition of the computation, $\theta_h = 1.0$, $0 \leqslant \Psi \leqslant 4.238$, $0 \leqslant \theta \leqslant 1.0$; and oscillatory solutions at (b) $\tau = 0$, $\theta_h = 1.0$, $0 \leqslant \Psi \leqslant 2.775$, $0 \leqslant \theta \leqslant 1.0$; (c) $\tau = 1/4\tau_p$, $\theta_h = 2.0$, $0 \leqslant \Psi \leqslant 7.886$, $0 \leqslant \theta \leqslant 2.0$; (d) $\tau = 2/4\tau_p$, $\theta_h = 1.0$, $-0.019 \leqslant \Psi \leqslant 5.449$, $0 \leqslant \theta \leqslant 1.318$; and (e) $\tau = 3/4\tau_p$, $\theta_h = 0$, $-0.145 \leqslant \Psi \leqslant 0.624$, $0 \leqslant \theta \leqslant 0.279$.

closure at larger inclined angles, heat transfer is enhanced and the duration time for response can thus be shortened.

Fig. 17 shows the influences of inclination on the averaged heat transfer at $Ra = 2000$ with and without imposed wall-temperature modulation. For this slightly supercritical condition with respect to a horizontal enclosure, the modulation at small inclined angles may provide a stabilizing effect to suppress the occurrence of the multi-cell motion in the enclosure. Therefore, the modulation effects for $\gamma \leqslant 3°$ alleviate the heat transfer rates as that shown in Fig. 17. For the cases of higher inclination, the cellular motion in the enclosure becomes strong enough. Bottom-wall temperature modulation cannot bring the flow field to a conduction-dominated state but turn to excite the flow oscillation. The heat transfer enhancement is thus presented and increased with the inclined angle. The modulation effect on heat transfer enhancement becomes saturated at large inclined angle.

5. Concluding remarks

The effects of bottom-wall temperature modulation on the threshold of thermal instability and the oscillatory cellular convection in a rectangular enclosure of aspect ratio 4:1 have been investigated numerically. From the present results the following conclusions can be drawn.

1. Bottom-wall temperature modulation of high amplitude and/or low frequency provides a stabilizing effect on the onset of thermal instability associated to the bifurcation of conduction-dominated state turning to convection one in a horizontal enclosure heated from below.

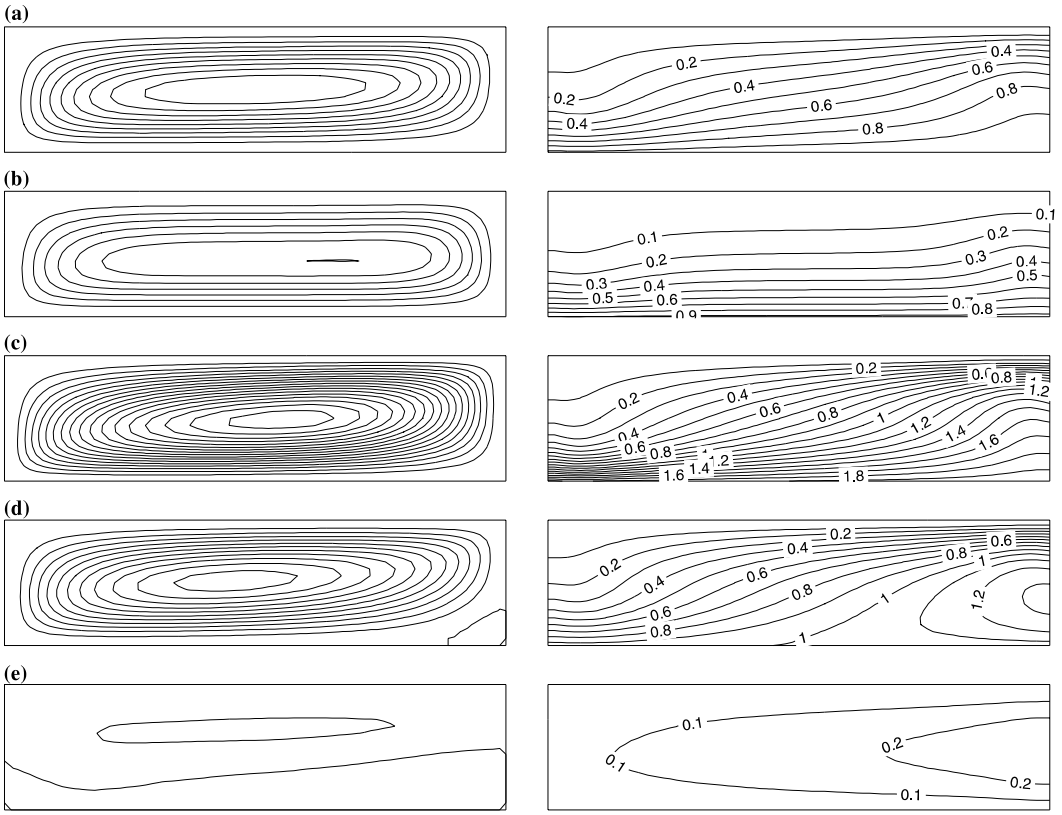

Fig. 13. Streamlines and isotherms for the case of $Pr = 0.71$, $Ra = 2000$, $\gamma = 90°$, $\varepsilon = 1.0$ and $\omega = 1.0$. (a) Steady state (SS) as initial condition of the computation, $\theta_h = 1.0$, $0 \leqslant \Psi \leqslant 4.965$, $0 \leqslant \theta \leqslant 1.0$; and oscillatory solutions at (b) $\tau = 0$, $\theta_h = 1.0$, $0 \leqslant \Psi \leqslant 3.505$, $0 \leqslant \theta \leqslant 1.0$; (c) $\tau = 1/4\tau_p$, $\theta_h = 2.0$, $0 \leqslant \Psi \leqslant 8.816$, $0 \leqslant \theta \leqslant 2.0$; (d) $\tau = 2/4\tau_p$, $\theta_h = 1.0$, $-0.047 \leqslant \Psi \leqslant 5.775$, $0 \leqslant \theta \leqslant 1.327$; and (e) $\tau = 3/4\tau_p$, $\theta_h = 0$, $-0.287 \leqslant \Psi \leqslant 0.558$, $0 \leqslant \theta \leqslant 0.286$.

Table 3
The flow structure in the enclosure with imposed modulation at different inclined angles[a]

γ	SS	τ			
		0	$1/4\tau_p$	$2/4\tau_p$	$3/4\tau_p$
1°	4C	0	2C	3C	3C
5°	3C	2in1C	2in1C	3C	3C, 2S
15°	2C	2in1C	2in1C	3C	3C, 2S
25°	2in1C	2in1C	2in1C	2in1C, 1S	2in1C, 2in1S and 1S
50°	2in1C	1C	1C	1C, 1S	1C, 2S
70°	1C	1C	1C	1C, 1S	1C, 2in1S
90°	1C	1C	1C	1C, 1S	1C, 2in1S

[a] C = cell; S = secondary vortices; SS = steady state; 2in1C = two-in-one cell; 2in1S = two-in-one secondary cell.

2. The flow structure and the isotherm pattern are altered periodically with the temperature modulation. The cyclic changes in flow structure and the number of cells are more remarkable at the lower inclined angles. At higher inclination angles, e.g., $\gamma \geqslant 50°$, the uni-cell flow structure is quite stable.

3. As the fluid temperature increases with the bottom-wall temperature, the convection velocity of the fluids raised up by the thermal buoyancy effect. Whereas the local fluid temperature approaches to be uniform around the trough of the oscillating bottom-wall temperature, the thermal buoyancy effect and, therefore, the strength of the cellular flow are diminished. These phenomena occur at the time instant of $\tau = 0.8\tau_p$.

4. In an inclined enclosure, time series of the local temperature show that the fluids around the corner of

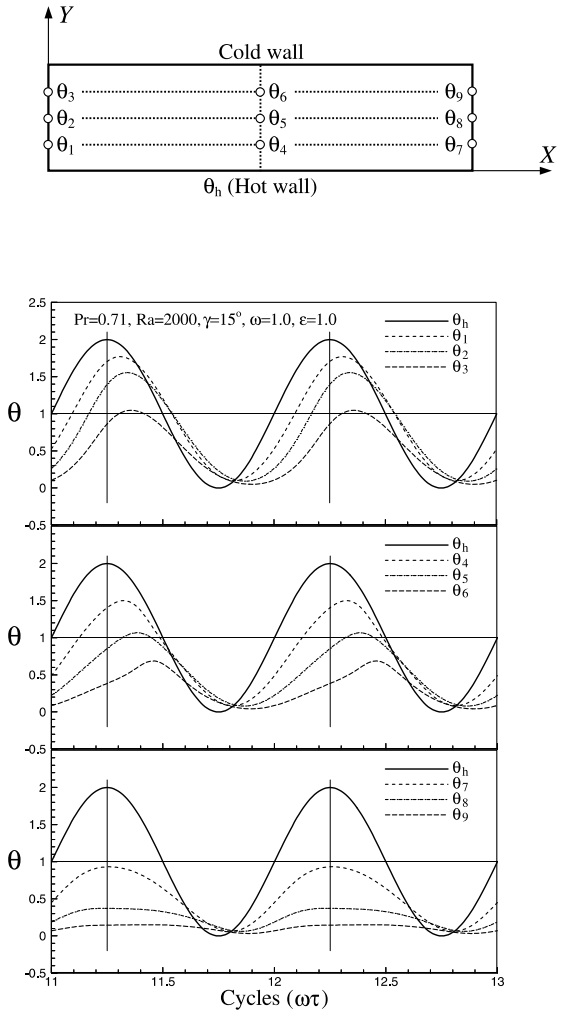

Fig. 14. Local temperature variations for $Pr = 0.71$, $Ra = 2000$, $\gamma = 15°$, $\varepsilon = 1.0$ and $\omega = 1.0$.

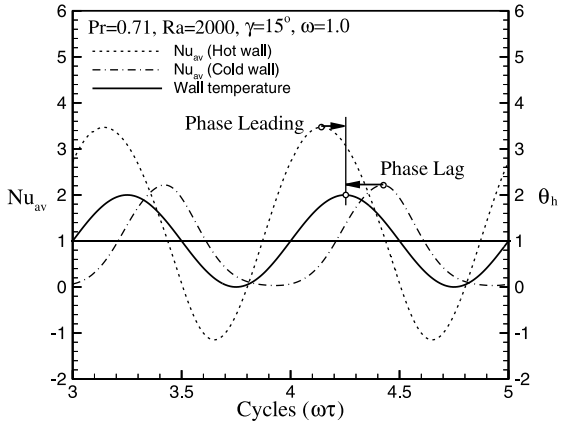

Fig. 15. Time variations of averaged heat transfer rates over the hot and cold walls for $Pr = 0.71$, $Ra = 2000$, $\gamma = 15°$, $\varepsilon = 1.0$ and $\omega = 1.0$.

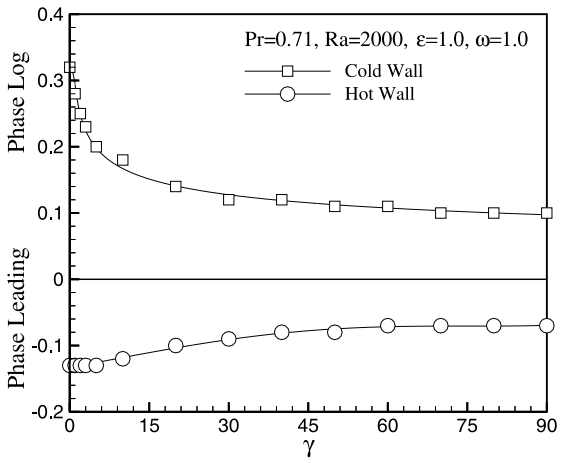

Fig. 16. Phase leading and lag of *Nu* responses at various inclined angles for $Pr = 0.71$, $Ra = 2000$, $\varepsilon = 1.0$ and $\omega = 1.0$.

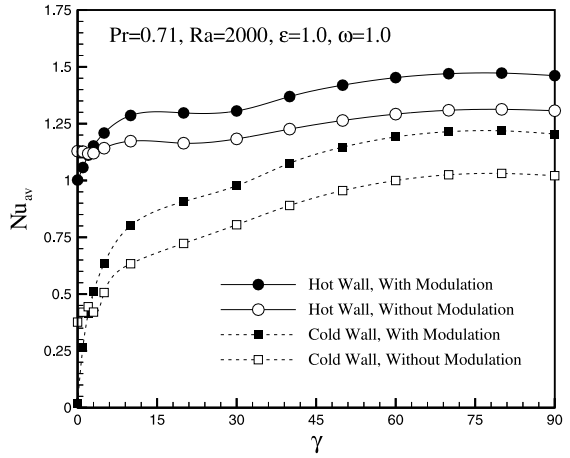

Fig. 17. Modulation effects on averaged Nusselt numbers at various inclined angles for $Pr = 0.71$, $Ra = 2000$, $\varepsilon = 1.0$ and $\omega = 1.0$.

hot wall of the lower-end side are of relatively larger amplitude and obvious phase lag; while the temperature responses on the high-end side-wall are almost in phase with the modulation.

5. It is found that the responses of both hot and cold walls are not in the same phase with that of the modulation. The cold wall responds with phase leading and the hot wall phase lag. The phase leading and lag of the heat transfer responses reduce with the increasing angle of inclination.

6. At higher angles, the heat transfer rate can be enhanced with imposed modulation. The fluid behaviors at $\gamma \leqslant 3°$ are more likely to the horizontal case, in which the modulation may suppress the onset of thermal instability and degrade the heat transfer rate. Out of this

range, the temperature modulation always enhances heat transfer and the enhancement seems to approach a saturate value.

References

[1] S. Ostrach, Natural convection in enclosures, ASME J. Heat Transfer 110 (1988) 1175–1190.

[2] K.T. Yang, Transitions and bifurcations in laminar buoyant flows in confined enclosures, ASME J. Heat Transfer 110 (1988) 1191–1204.

[3] J. Patterson, J. Imberger, Unsteady natural convection in a rectangular cavity, J. Fluid Mech. 100 (1980) 65–86.

[4] V.F. Nicollete, K.T. Yang, J.R. Lloyd, Transient cooling by natural convection in a two-dimensional square enclosure, Int. J. Heat Mass Transfer 28 (1985) 1721–1732.

[5] S.D. Schladow, J.C. Patterson, R.L. Street, Transition flow in a side-heated cavity at high Rayleigh number: a numerical study, J. Fluid Mech. 200 (1989) 121–148.

[6] H.Q. Yang, K.T. Yang, Q. Xia, Periodic laminar convection in a tall vertical cavity, Int. J. Heat Mass Transfer 32 (11) (1989) 2199–2207.

[7] M. Kazmierczak, Z. Chinoda, Buoyancy-driven flow in an enclosure with time periodic boundary conditions, Int. J. Heat Mass Transfer 35 (6) (1992) 1507–1518.

[8] J.L. Lage, A. Bejan, The resonance of natural convection in an enclosure heated periodically from the side, Int. J. Heat Mass Transfer 36 (8) (1993) 2027–2038.

[9] J.M. Hyun, Unsteady buoyant convection in an enclosure, Adv. Heat Transfer 34 (1994) 277–320.

[10] Q. Xia, K.T. Yang, D. Mukutmoni, Effect of imposed wall temperature oscillations on the stability of natural convection in a square enclosure, ASME J. Heat Transfer 117 (1995) 113–120.

[11] H.S. Kwak, J.M. Hyun, Natural convection in an enclosure having a vertical sidewall with time-varying temperature, J. Fluid Mech. 329 (1996) 65–88.

[12] G. Venezian, Effect of modulation on the onset of thermal convection, J. Fluid Mech. 35 (1969) 243–254.

[13] S. Rosentblat, D.M. Herbert, Low-frequency modulation of thermal instability, J. Fluid Mech. 43 (1970) 385–398.

[14] S. Rosentblat, G.A. Tanaka, Modulation of thermal convection instability, Phys. Fluids 14 (7) (1971) 1319–1322.

[15] R.G. Finucane, R.E. Kelly, Onset of instability in a fluid layer heated sinusoidally from below, Int. J. Heat Mass Transfer 19 (1976) 71–85.

[16] S.H. Davis, The stability of time-periodic flows, Annu. Rev. Fluid Mech. 8 (1976) 57–74.

[17] G. Ahlers, P.C. Hohenberg, M. Lucke, Externally modulated Rayleigh–Benard convection: experiment and theory, Phys. Rev. Lett. 53 (1) (1984) 48–51.

[18] M.N. Roppo, S.H. Davis, S. Rosentblat, Benard convection with time-periodic heating, Phys. Fluids 27 (4) (1984) 796–803.

[19] J. Mantle, M. Kazmierczak, B. Hiawy, The effect of temperature modulation on natural convection in a horizontal layer heated from below: high-Rayleigh-number experiments, ASME J. Heat Transfer 116 (1994) 614–620.

[20] J.L. Lage, B.V. Antohe, Convection resonance and heat transfer enhancement of periodically heated fluid enclosures, in: J. Padet, F. Arinc (Eds.), in: Transient Convective Heat Transfer, Begell House, New York, 1997, pp. 259–268.

[21] C.Y. Soong, P.Y. Tzeng, T.S. Sheu, Influences of initial and boundary conditions on numerical solutions of laminar natural convection in enclosures, in: C. Taylor, P. Durbetaki (Eds.), Numerical Methods in Laminar and Turbulent Flow, vol. 9, Part 1, Pineridge Press, UK, 1995, pp. 656–665.

[22] C.Y. Soong, P.Y. Tzeng, D.C. Chiang, T.S. Sheu, Numerical study on mode-transition of natural convection in differentially heated inclined enclosures, Int. J. Heat Mass Transfer 39 (6) (1996) 1507–1518.

[23] P.Y. Tzeng, C.Y. Soong, T.S. Sheu, Numerical investigation of transient flow-mode transition of laminar natural convection in an inclined enclosures, Numer. Heat Transfer A 31 (1997) 193–206.

[24] T. Hayase, J.A.C. Humphrey, R. Greif, A consistently formulated QUICK scheme for fast and stable convergence using finite-volume iterative calculation procedures, J. Comp. Phys. 98 (1992) 108–118.

[25] P. van Doormaal, G.D. Raithby, Enhancements of SIMPLE method for predicting incompressible fluid flow, Numer. Heat Transfer (7) (1984) 147–163.

[26] B. Roux, Numerical simulation of oscillatory convection in low-*Pr* fluids, A GAMM Workshop, Friedr. Vieweg and Sohn Verlagsgescllschaft mbH, Braunschweig, 1990.

[27] J. Zierep (Ed.), Convective Transport and Instability Phenomena, G. Braum, GmbH, Karlsruhe, Germany, 1982.

[28] R.J. Donnelly, K.W. Schwart, Experiments on the stability of viscous flow between rotating cylinders, Proc. R. Soc. Lond. A 208 (1965) 531–546.